Songklanakarin J. Sci. Technol.
45 (4), 501–509, Jul. – Aug. 2023

http://www.sjst.psu.ac.th

*Original Article*

# Opal-CT from the Lam Narai Volcanics in Lop Buri, Thailand: Mineralogy and petrogenesis

Pimwaree Thitiwatthanakarn[1*], Supanut Suntikoon[2], and Chanakan Wisessan[1]

[1] *Department of Geological Sciences, Faculty of Science, Chiang Mai University, Mueang, Chiang Mai, 50200 Thailand*

[2] *Environmental Science Research Center, Faculty of Science, Chiang Mai University, Mueang, Chiang Mai, 50200 Thailand*

Received: 25 December 2022; Revised: 3 April 2022; Accepted: 30 June 2023

## Abstract

Common opal comes in a variety of colors including green, orange, red, yellow, and white. The specific gravity of the samples ranges from 1.83 to 1.95. The refractive index ranges from 1.44 to 1.45. According to the Fourier-transform infrared results, the absorption bands ranging from 4000 to 400 $cm^{-1}$ are related to lattice vibration. There are absorption bands at 3400, 1630, 1095, 793, 621, and 479 $cm^{-1}$. The results of X-ray diffraction used to identify and/or characterize crystal structure indicate identification as opal-CT. To determine the nature of chemical impurities, samples were analyzed using inductively coupled plasma - mass spectrometry after dilution. The results are related to the mode of formation and physical properties, and they help to define the geographical origin. Rock samples are silicic in composition and show a sub-alkaline magma series, whereas volcanic rock samples are rhyolite. The REE patterns of opals and rocks are parallel. As a result, the opals are genetically related to their host rocks. The Ba content is critical in distinguishing volcanic opal from sedimentary opal. Because the Ba level is below 110 ppm, the sample is from a volcanic environment.

**Keywords**: common opal, opal-CT, origin, mineralogy, petrogenesis

## 1. Introduction

Opal has the chemical formula $SiO_2.nH_2O$. The absence of crystallinity in opal results in the peculiar optical phenomenon known as opalescence (Marlow, Sharifi, Brinkmann, & Mendive, 2009). According to their structure and crystallinity, opals are divided into three categories: opal-A for amorphous opal, opal-CT for opals with disordered cristobalite and tridymite stacking, and opal-C for opals with cristobalite. Opals are categorized genetically into three groups: volcanic, sedimentary, and volcano-sedimentary. A sedimentary opal is created by precipitates from silicic fluid in cracks in weathered silicic rocks (Vysotsky *et al*., 2010; Vysotskiy, Ignatiev, Khlestunova, Velivetskaya, & Okrugin, 2013). In order to distinguish between volcanic and sedimentary opals, Ba is crucial. Ba content in volcanic opals is less than 110 ppm (Chauviré *et al*., 2019).

Physical characteristics like color are affected by the quantities of trace elements. The causes of color can be understood by looking at the geochemical differences between various color opals, paleness, and by comparing precious and common opal. Common opal colors are influenced by two main factors: the first is attributed to diffraction, e.g., the size of silica spheres causes coloration as green or blue with small spheres, red (fire opal) with larger sized spheres; and secondly by mineral inclusions and chemical impurities, as for instance green, blue, and pink opals have larger concentrations of trace elements (impurities) than those of other colors (Mg and Cu for green and blue opal, Mn – rather than Mg – and Al for pink opals). Austrian opaque opals are tinted orange by the presence of realgar. Pink opals are found to have inclusions of

*Corresponding author
Email address: pimwaree_t@cmu.ac.th

palygorskite (phyllosilicate) and organic substances (Caucia, Marinoni, Leone, & Ghisoli, 2015). Orange opal (yellow to orange to red to chocolate-brown color) are found to contain nano-inclusions of iron-containing products such as Fe-oxyhyoxides (Meier, Ungerer, Klinge, & Nirschl, 2018).

One of the significant places in Thailand to research the genesis processes of hypothetical volcanic opals is Lop Buri, which features opal deposits linked to the Lam Narai Volcanics. Common opals and varieties of quartz including chalcedony, quartz, and agate have been extracted from *in situ* soil or basalt and rhyolitic tuff rubble. The volcanic succession in this area is composed of Late Cenozoic basaltic flows, Tertiary andesite, rhyolite and rhyodacite, and Upper Permian-Lower Triassic andesite porphyry.

The primary objectives of this study are to elucidate the modes of occurrence of opal on the basis of trace element chemistry, and to clearly understand the chemical composition as it is related to the opal structure.

## 2. Methodology

### 2.1 Geology of Lam Narai Volcanics, Lop Buri province

The Lam Narai Volcanics are a component of a Late Cenozoic volcanic sequence in central Thailand that stretches from Phetchabun to Nakhon Nayok Province (Figure 1). Among the rocks found in this area are basaltic andesite, andesite and rhyolite, tuff, and agglomerate. These rocks are separated into three sections: Phetchabun, Lam Narai, and Saraburi-Nakhon Nayok. According to Jungyusuk and Suriyachai (1987), the volcanic rocks that make up the Lam Narai section range from basic to acidic. The oldest rocks were andesite porphyry, basaltic andesite, quartz latite, and quartz trachyte. These rocks were buried in Tertiary acidic pyroclastic deposit, with Quaternary basalt covering the highest layer. In the Lam Narai district of Lop Buri, vast deposits of rhyolite, glassy breccia, pitchstone perlite, and pyroclastic material are also covered by the basaltic flow (Janyawanich, 1987).

The Cenozoic volcanic rock at Lop Buri was formed by eruptions of olivine tholeiitic and alkalic basalt, trachyandesite, dacite, and rhyolite in the Late Tertiary and Quaternary (Barr & Cooper, 2013). The Chao Phraya Plain's rhyolite was dated to 22.5 Ma. K/Ar dating was used to determine the dates of the basalts from Khok Samrong, which were 11.29±0.64 Ma. Locally, the eruption of acidic magma produced a layered structure with large rhyolite layers on top and glassy strata with pyroclastic rock layers at the bottom. Most of the low terrane plain was covered in basalt lava flows.

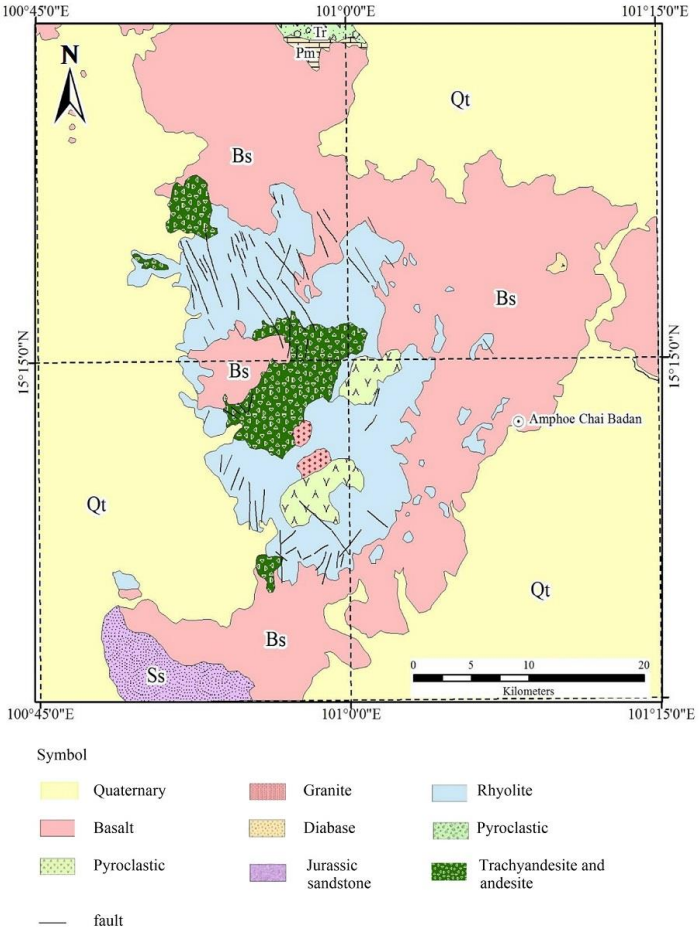


Figure 1. Geological map of the Lam Narai area shows distribution of rock types, with study areas represented by bold squares. Lines present topographic map sheet (scale 1:50,000) at right top corner (modified from (Intasopa, 1995)).

### 2.2 Materials

Fifty-five common opals were used in the analysis. Based on color, the samples were divided into four groups: multi-colored and green; red; orange and yellow; and white. Further, 9 rock samples were used to establish genetic relationship between opals and their host rocks by using X-ray fluorescence spectrometry (XRD) for major oxides and inductively coupled plasma mass spectrometry (ICP-MS) for trace and rare earth elements.

### 2.3 Equipments

The following instruments were utilized for analyzing the mineralogical properties of the samples: a hydrostatic balance to determine specific gravity, a polariscope to differentiate between isotropic and anisotropic substances, a refractometer to determine refractive index and birefringence, an ultraviolet lamp to observe fluorescence, a gemological microscope to observe internal features, and a GIA GemSet to grade the color.

Non-destructive Fourier-transform infrared spectroscopy was used to investigate the vibrational absorption properties of materials. Powdered opal samples were combined with KBr and pressed into discs. The samples were measured at room temperature and then purged with liquid nitrogen. Infrared spectra in the range of 4000 to 400 $cm^{-1}$ were obtained using a spectrometer fitted with a transmittance attachment, with a standard resolution of 4 $cm^{-1}$ and 120 scans per second, at the Faculty of Science and Technology, Chiang Mai Rajabhat University, Thailand. To demonstrate the linear relationship between the optical path length and sample thickness, all spectra were saved in absorbance mode.

Crystal structure was determined and/or characterized using X-ray diffraction. A BrukerD8Advance diffractometer equipped with a copper X-ray tube, at Chiang Mai University, was used to conduct the XRD analysis on powdered samples.

The study used Inductively Coupled Plasma Mass Spectrometry (ICP-MS) to identify trace and rare earth elements. Three powdered opal samples were prepared. Prior to digestion using Berghof Company's Microwave Digestion: SW-X, the 100 mg sample was dissolved in 2.5 ml of 65% nitric acid and 1 ml of 40% hydrofluoric acid. The solution was then analyzed using an ICP-MS iCAP Q from Thermo Fisher Scientific Company. All samples in this analysis were analyzed at the Synchrotron Light Institute (Thailand).

Scanning Electron Microscopy with Energy Dispersive X-ray Fluorescent Spectrometry (SEM-EDS) is a non-destructive method for chemical and textural analysis. The samples required a gold coating to be electrically conductive. The results were obtained using a JEOL Model: JSM-5900LV scanning electron microscope and Oxfords' INCA software, at Chiang Mai University.

## 3. Results and Discussion

### 3.1 Common opals

Fifty-five common opals were divided into four classes. Table 1 lists the mineralogical properties of common opal. Some common opal specimens have an internal layer of color, which is filled with orangey yellow stains from iron oxide in internal fractures and an orange line. Many samples have mottled and orange color zoning.

FTIR absorption bands were present in all groups at 3400, 1630, 1095, 793, 621, and 479 $cm^{-1}$ (Figure 2). O-Si-O and Si-O-Si bending, and Si-O asymmetric stretching vibrations are responsible for the bands at 470, 796, and 1100 $cm^{-1}$. The absorption peak at 1100 $cm^{-1}$ (Chauviré, Rondeau, & Mangold, 2017) confirms the formation of a network structure within the opal. The H-O-H bending vibrations of molecular water related to two water species, $H_2O$ and SiOH group, causing the peak around 1600 $cm^{-1}$. The Si-OH group is responsible for the absorption band at 3400 $cm^{-1}$.

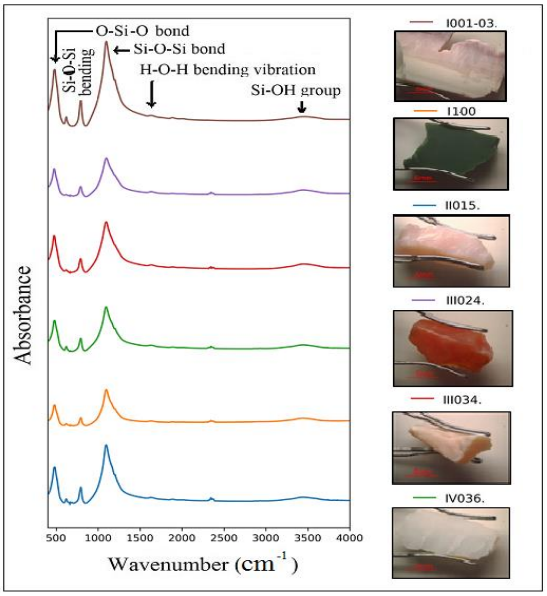


Figure 2. Infrared absorption spectra of opals show absorption bands at 3400, 1630, 1095, 793, 621, 479 $cm^{-1}$

Table 1. Mineralogical properties of common opal samples from Lop Buri

| Properties | Group I | Group II | Group III | Group IV |
|---|---|---|---|---|
| Color | three-color (purple, red and yellow) and green | Red | Orange and yellow | White |
| Interference figure | - | - | - | - |
| Specific gravity | 1.820-1.922 | 1.830-1.890 | 1.920-1.950 | 1.870-1.880 |
| Refractive index | 1.44-1.45 | 1.44-1.45 | 1.44-1.45 | 1.44-1.45 |
| UV Fluorescence | | | | |
| Short-wave UV | inert | inert | inert | inert |
| Long-wave UV | inert | inert | inert | inert |

- = not observed

From SEM-EDS, the results are shown in Table 2. Lop Buri opal had high levels of silica oxide. There are trace elements (impurities) substituted for $Si^{4+}$. In a purple layer the samples had higher levels of $Al_2O_3$. The $Al^{3+}$ is one impurity causing coloration. In red- and yellow-layer, samples had higher $Fe_2O_3$, with $Fe^{3+}$ causing orange, red or yellow coloration (Devès *et al*., 2012). In green sample, the composition had $SiO_2$ 81.508 wt.%, $Al_2O_3$ 10.271 wt.%, $Fe_2O_3$ 1.96 wt.%, $K_2O$ 6.261wt% in XRF results. Green coloration is caused by Al elements (Caucia *et al*., 2015). Fe impurity in group III is higher than in group II, thus SG in group III is higher because Fe causes SG to increase. Al and K impurities are higher in group IV than in group III. Milky opal coloration depends on Al and K impurities (Devès *et al*., 2012). The Ba content in all samples (Table 3) was less than 110 ppm, so the source of these opal samples can be classified as volcanic rock.

Table 2. Major and minor oxides in common opal analyzed by SEM-EDS (wt%).

| % oxide sample | Group I | | | Group II | | |
|---|---|---|---|---|---|---|
| | OP001-1 | OP001-2 | OP001-3 | OP012 | OP015 | OP 019 |
| $SiO_2$ | 97.61 | 98.7 | 98.83 | 95.64 | 99.01 | 97.99 |
| $Al_2O_3$ | 1.05 | 0.27 | 0.26 | 3.69 | 0.37 | 1.82 |
| $Fe_2O_3$ | 0 | 0.19 | 0.23 | 0 | 0.09 | 0 |
| CaO | 0.12 | 0.37 | 0.22 | 0 | 0.11 | 0.02 |
| $Na_2O$ | 0.22 | 0.46 | 0.27 | 0.55 | 0.17 | 0.11 |
| $K_2O$ | 0.86 | 0 | 0.18 | 0.12 | 0.25 | 0.07 |
| LOI | 1.25 | 1.25 | 1.25 | 1.95 | 1.76 | 1.89 |
| Total | 101.11 | 101.24 | 101.24 | 101.95 | 101.76 | 101.90 |

Table 2. Continued.

| % oxide sample | Group III | | | | Group IV | | | | |
|---|---|---|---|---|---|---|---|---|---|
| | OP024 | OP026 | OP029 | OP133 | OP163 | OP038 | OP040 | OP042 | OP184 |
| $SiO_2$ | 98.96 | 98.56 | 97.77 | 91.77 | 99.78 | 98.58 | 99.2 | 98.55 | 99.47 |
| $Al_2O_3$ | 0.73 | 0.46 | 0.82 | 4.05 | 0 | 0.84 | 0.34 | 0.84 | 0.1 |
| $Fe_2O_3$ | 0.16 | 0.12 | 0.62 | 0.70 | 0 | 0 | 0 | 0.16 | 0 |
| CaO | 0.18 | 0.52 | 0.02 | 2.88 | 0.04 | 0.19 | 0 | 0.08 | 0 |
| $Na_2O$ | 0 | 0.19 | 0.48 | 0.05 | 0.09 | 0.3 | 0.21 | 0.17 | 0.19 |
| $K_2O$ | 0.38 | 0.15 | 0.29 | 0.55 | 0.09 | 0.09 | 0.24 | 0.21 | 0.24 |
| LOI | 2.05 | 2.56 | 1.69 | 1.89 | 2.03 | 1.84 | 1.96 | 2.12 | 1.64 |
| Total | 102.46 | 102.56 | 101.69 | 101.89 | 102.03 | 101.84 | 101.95 | 102.13 | 101.64 |

Table 3. Rare earth and trace element concentrations determined by ICP-MS (ppm).

| Element | Opal | | | Rock | | |
|---|---|---|---|---|---|---|
| | OP163 | OP038 | OP184 | R001 | R004 | R007 |
| Na | 137.25 | 340.07 | 447.80 | 36,035.28 | 48,389.14 | 43,684.53 |
| Mg | 140.18 | 207.52 | 121.48 | 237.79 | 168.90 | 219.66 |
| Al | 2,014.69 | 4,302.51 | 2,343.06 | 10,399.02 | 6,661.14 | 16,666.33 |
| K | 494.01 | 572.54 | 904.73 | 43,536.67 | 47,180.45 | 48,635.23 |
| Ca | 64.76 | 188.52 | 128.34 | 237.29 | 396.98 | 248.94 |
| SC | 2.65 | 3.19 | 2.59 | 3.88 | 4.92 | 4.92 |
| Ti | 2.78 | 11.08 | 7.71 | 1,090.40 | 2,080.29 | 2,059.76 |
| V | 0.27 | <LOD | <LOD | 12.20 | 23.95 | 20.53 |
| Cr | 0.55 | 2.78 | 6.59 | 7.50 | 6.39 | 5.53 |
| Mn | 18.20 | 21.88 | 17.91 | 184.31 | 224.76 | 157.40 |
| Fe | 110.64 | 51.89 | 32.05 | 4,956.06 | 4,875.02 | 9,093.80 |
| Co | 0.59 | 0.61 | 0.58 | 74.68 | 65.42 | 70.47 |
| Ni | 7.81 | 6.08 | 10.49 | 13.27 | 9.95 | 9.34 |
| Cu | 9.10 | 14.38 | 2.51 | 3.19 | 4.75 | 3.25 |
| Zn | 4.40 | 13.80 | 12.24 | 22.48 | 37.56 | 28.03 |
| As | 1.44 | 0.42 | 0.42 | 5.38 | 7.21 | 5.52 |
| Rb | 4.52 | 5.54 | 10.99 | 104.98 | 89.88 | 82.25 |
| Sr | 6.01 | 10.57 | 13.33 | 47.04 | 149.04 | 148.03 |
| Y | 9.47 | 0.36 | 0.40 | 34.10 | 34.72 | 33.37 |

Table 3. Continued.

| Element | Opal | | | Rock | | |
|---|---|---|---|---|---|---|
| | OP163 | OP038 | OP184 | R001 | R004 | R007 |
| Zr | 2.98 | 2.95 | 4.92 | 139.60 | 574.50 | 384.53 |
| Nb | 2.32 | 2.28 | 2.32 | 18.64 | 26.84 | 23.88 |
| Cd | 0.04 | 0.04 | 0.03 | 0.09 | 0.10 | 0.08 |
| Cs | 3.57 | 11.27 | 15.83 | 4.09 | 6.18 | 6.30 |
| Ba | 14.60 | 22.91 | 25.25 | 638.93 | 845.71 | 664.25 |
| La | 0.76 | 0.70 | 0.70 | 4.12 | 5.03 | 4.03 |
| Ce | <LOD | <LOD | <LOD | 9.97 | 18.19 | 12.09 |
| Pr | <LOD | <LOD | <LOD | 0.56 | 0.78 | 0.60 |
| Nd | 0.27 | 0.20 | 0.18 | 1.97 | 2.58 | 3.26 |
| Sm | <LOD | <LOD | <LOD | 0.87 | 0.96 | 0.86 |
| Eu | 0.05 | 0.05 | 0.05 | 0.10 | 0.16 | 0.15 |
| Gd | 0.45 | 0.35 | 0.35 | 0.70 | 0.85 | 0.76 |
| Tb | <LOD | <LOD | <LOD | <LOD | <LOD | <LOD |
| Dy | 0.74 | 0.55 | 0.56 | 0.99 | 1.13 | 1.02 |
| Ho | 0.15 | 0.11 | 0.11 | 0.21 | 0.24 | 0.21 |
| Er | 0.79 | 0.66 | 0.67 | 0.99 | 1.07 | 0.97 |
| Tm | <LOD | <LOD | <LOD | <LOD | <LOD | <LOD |
| Yb | 0.47 | 0.44 | 0.46 | 0.84 | 0.89 | 0.79 |
| Lu | 0.07 | 0.08 | 0.09 | 0.14 | 0.15 | 0.13 |
| Pb | <LOD | 0.47 | <LOD | 6.87 | 16.18 | 6.31 |
| Th | <LOD | <LOD | <LOD | 20.98 | 20.86 | 20.51 |
| U | 3.96 | <LOD | <LOD | 0.92 | 0.54 | 0.19 |
| Selected element ratios | | | | | | |
| La/Sm | - | - | - | 4.74 | 5.24 | 4.68 |
| Sm/Yb | - | - | - | 1.04 | 1.08 | 1.09 |
| La/Yb | 1.6 | 1.59 | 1.52 | 4.90 | 5.65 | 5.10 |

LOD = Limit of detection, - = not analyze

The XRD result for opal-CT is characterized by three broad reflections: 1) the most intense of which occurs at about 4.12 to 4.05Å (21.74 to 22.00$^{O}$ 2θCuK.), 2) a subsidiary peak or shoulder at about 4.32Å (20.72$^{O}$), and 3) a weaker reflection at about 2.50Å (35.90$^{O}$) (Wilson, 2014). All the opal samples showed peaks at 4.12 to 4.05Å (21.74 to 22.00$^{O}$ 2θCuK.), 4.32Å (20.72$^{O}$) and 2.50Å (35.90$^{O}$). Then, all the samples are identified as opal-CT. Some samples had peaks at 3.34Å attributed to quartz (Figure 3).

In SEM analysis all the opal samples showed morphology with agglomerates, and fibrous, platelet, and tablet textures (Figure 4). Opal samples consisted of aggregates with variable shapes and sizes. Silica spheres were formed aggregates with a near-spherical shape. For example, in op100, 012, and 038, layers formed by the combination of silica spheres were found. The layers were arranged parallel to each other. The agglomerates formed by silica spheres are scattered in the layers, with diameters of about 100-400 nm. Silica aggregates of various shapes (spherical, long stick, fibrous, platelet, tablet, etc.; 100 to 400 nm diameter) and a disorderly accumulation were observed on op012, 133, and 100. The silica aggregates formed irregular-shaped agglomerates. The irregularity of the spheres, which is present in the majority of naturally occurring opals, is related to the instability of the geological environment. The silica spheres are easily agglomerated in the hydrothermal environment when the temperature is high; nevertheless, they are arranged in a predictable way when the temperature and pressure are stable (Luo, Liu, & Yang, 2016). All samples showed agglomerate spheres, indicating that the occurrence of opal was related to hydrothermal environment.

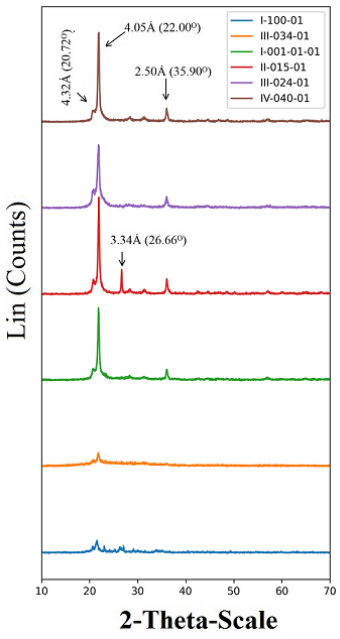


Figure 3. Opal samples had cristobalite, tridymite and quartz according to XRD results.

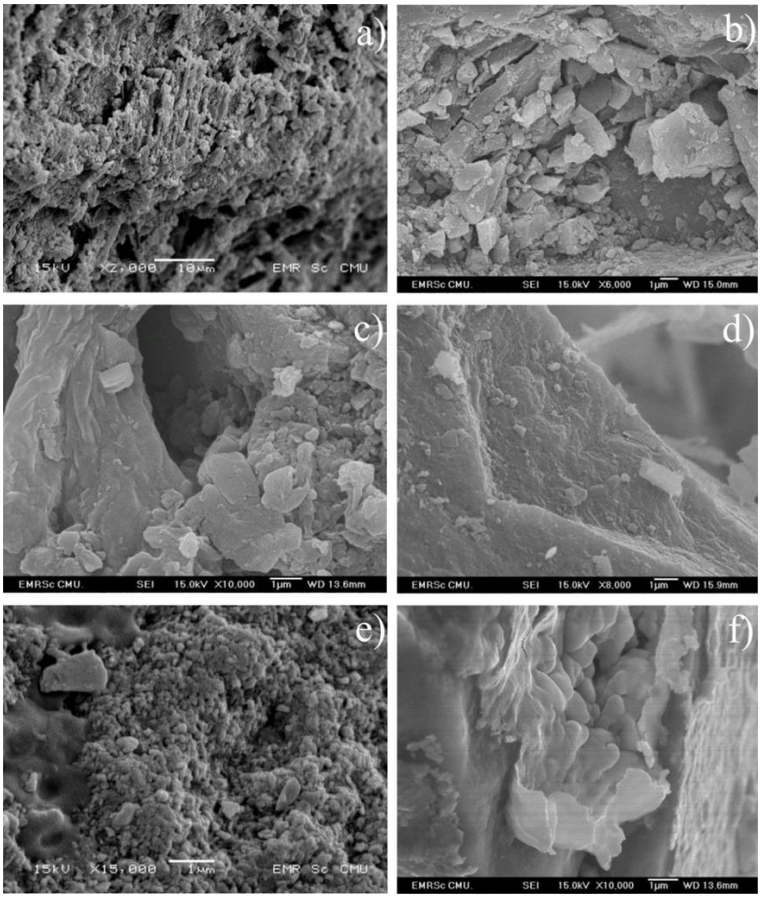


Figure 4. Layers and aggregates observed by SEM; a) Op 100 (Group I) shows structure built from bundles of fibers (diameters 250-2500 nm), b) Op 012 (Group II) shows silica aggregates, c) Op 133 (Group III) shows silica aggregates of various shapes such as tablet (diameters 120-700 nm) and pore, d) Op 038 (Group IV) shows a layered structure, e) Small spheres of op 100 with diameters of 100-400 nm, and f) silica spheres of Op 026 (Group III) with diameters of 200-300 nm

## 3.2 Rocks

### 3.2.1 Lithology and petrography

Megascopic characters: the rock is brownish red to red color, with porphyritic texture. There is plagioclase phenocryst usually shown in tabular or platy shape, of which sizes are up to 1.00-2.00 mm across, and normally formed by alignment texture. There is high weathering in the surface in brown to brownish red color. The samples of rhyolite were frequently cross-cut by opal in small veins. Opal was found in vesicles and fracture fillings.

Microscopic characters: the fine-grained rock samples are moderately porphyritic rocks. The phenocryst/microphenocryst assemblages include plagioclase/K-feldspar + biotite ± opaque mineral. The phenocrysts/microphenocrysts are made up mainly of plagioclase with subordinate biotite and muscovite.

Plagioclase phenocrysts (Figure 5) are generally anhedral to subhedral with sizes up to 0.5-1.5 mm across, having zonal patterns and polysynthetic twins. Plagioclase show rounded edges, embayed outlines and sieve textures. Some crystal may be replaced by clay mineral and sericite.

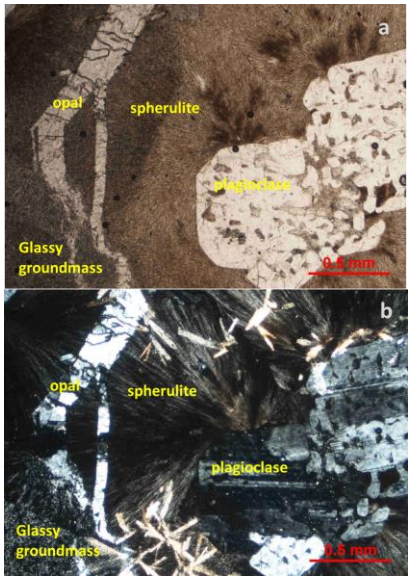


Figure 5. R 004 thin section shows porphyritic texture, glassy groundmass and plagioclase; a. ordinary light, b. crossed polarizing filters.

K-feldspar phenocrysts are commonly anhedral to subhedral, showing rounded edges and rare embayment. Some crystal may be replaced by clay mineral.

Biotite phenocrysts are subhedral to euhedral. Some biotite flakes are slightly replaced by Fe-Ti oxide and hematite/iron oxide.

Opaque microphenocryst shows anhedral to subhedral outlines. These minerals are both of primary and secondary minerals.

The groundmass is mostly glassy and has partly undergone high temperature devitrification and low temperature recrystallization. In general, the groundmass constituents are largely plagioclase, and minor components of biotite, spherulite and opal. Samples have spherulitic groundmass with diameters up to 0.5-4 mm that are the result of high temperature devitrification. The spherulitic growth was divided into a large spherulite and an isolated spherulite. The isolated spherulite has nucleated on pre-existing phenocryst as plagioclase. Secondary mineral is opal normally found in rock samples. Tiny fractures or veins are sealed with opal. Some groundmass is mosaic of fine quartz and feldspar.

### 3.2.2 Major and minor oxides, and trace and rare earth elements

The bulk chemical compositions of the opal bearing rocks were 76.69-81.65 wt% $SiO_2$, 0.16-0.32 wt%$TiO_2$, 10.37-13.72 wt%$Al_2O_3$, 0.84-1.60 wt%$Fe_2O_3$, 0.35-0.40 wt%MgO, 0.38-0.60 wt%CaO, 3.95-4.94 wt%$K_2O$, 1.33-2.10 wt%$Na_2O$, 0.00-0.06 wt%$P_2O_5$ and LOI 0.37-0.70 wt%. Rare earth and trace elements are shown in Table 3. As Si-oxide was the highest, these rocks are of silicic composition.

### 3.2.3 Magmatic affinities and rock types

The primary compositions of volcanic rock samples are compositionally basic, and acidic as evidenced by relationship between alkali and silica on the sum of the $Na_2O$ and $K_2O$ versus silica content as wt.%, and plot in the diagram for volcanic igneous rocks (Figure 6) suggests that all samples also fall in the rhyolite field. The sub-alkaline series in felsic rocks is supported by their concentrations of $Na_2O$ and $K_2O$ and silica content (Irvine & Baragar, 1971). These rocks trends in major and trace element variation diagrams can provide potential constraints on the nature of differentiation processes.

Chondrite-normalized REE patterns for three rhyolite samples are shown in Figure 7. The REE patterns for rhyolite show slightly light REE (for short LREE) enrichment with chondrite-normalized La/Sm varying from 4.68 to 5.24 and relatively flat heavy REE with chondrite-normalized Sm/Yb ranging from 1.04 to 1.09. The chondrite-normalized La/Yb of samples is 4.90-5.65. Rhyolite pattern shows Eu negative anomaly cause of plagioclase fractionation to correspond, and shows in rocks corrected in field and thin section in the study.

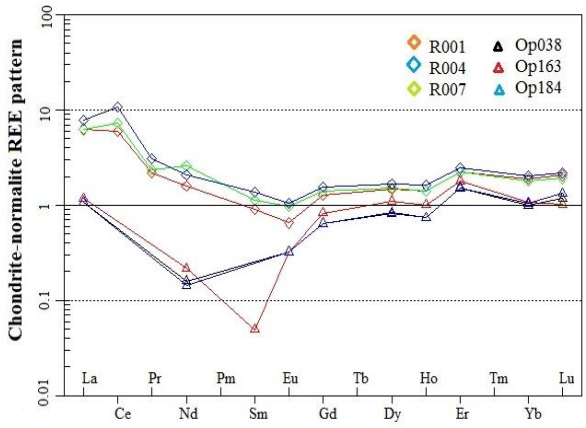


Figure 7. Chondrite-normalized REE diagram of Lop Buri opal and Rhyolite (McDonough and Sun, 1995)

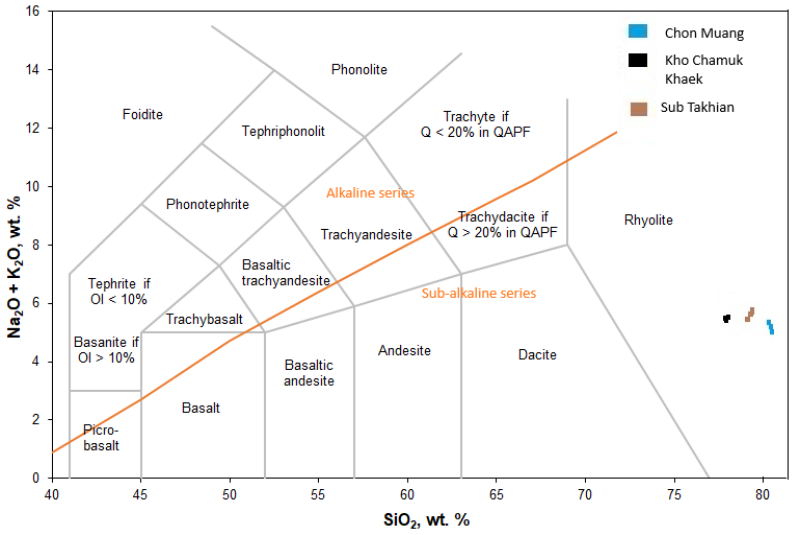


Figure 6. Plot of modified SiO2 versus ($Na_2O$+$K_2O$) in classification diagram (after BAS *et al.* (1986)) showing that the majority of Lop Buri rock samples were of felsic type and the subdivision of volcanic rock into alkaline and sub alkaline (tholeiitic) on a total alkalis versus silica. Diagram taken from Irvine and Baragar (1971).

### 3.3 Petrogenesis of opal

From chemical analyses, the host rock is silicic rock (rhyolite). Opal is found in fractures or veins of rhyolite. The sizes of opal samples are related with the sizes of cavities. The vesicles within rock were formed as a result of degassing and expansion of gas bubbles during rise of magma. Many gases escaped. However, gas bubbles were trapped in the cool outer lava layer (Moxon, 1996). The factors that caused variations in cavity size, shape and abundance in the rock are original magma volatile content and viscosity, rate of decompression and diffusion, and deformation during flow (Vona & Romano, 2013). These factors caused different cavity sizes. The spherulitic texture in rhyolite is characteristic of high temperature devitrification found in glassy lava. Watkins, Manga, Huber and Martin (2009) reported that the cavity begins as an initial vapor bubble in the host rhyolite contributed by devitrification of rhyolite or crystallization of spherulite. Devitrification of rhyolite or crystallization of spherulite can indicate increasing vapor pressure. The volatile became immiscible and was exsolved as an aqueous vapor, which condensed to form a hollow.

Opal forms either in volcanic or sedimentary deposits. It is believed to come from the weathering of silicic rocks such as rhyolite or sandstone, followed by precipitation from $SiO_2$-enriched liquid in cavities (Gaillou *et al*., 2008). Opal is not a pure form silica as it contains water component, and some impurities and trace elements can also enter in its structure.

The trace element chemistry of opal and its host rock can be indicated in a Chondrite-normalized diagram. Other opal/host rock patterns exhibit the same behavior. The shapes of host rock and opal patterns are similar (Devès *et al*., 2012). Figure 7 shows opal and rhyolite pattern. The chondrite-normalized La/Yb value of rock samples (4.90-5.65) is different from opal samples (1.52-1.60). The data indicate that the opals are genetically related to their host rocks (rhyolite). Opal is a secondary mineral filling in the cavities of host rock. The initial silica required for opal formation may have been infiltrated through the underlying high-silica volcanic rock and precipitated in the hollow from hydrothermal fluids. The mineral textures and forms suggest that the precipitation occurred at a low temperature (up to 170 $^{O}$C) (Caucia *et al*., 2015). The type of hydrothermal fluid is meteoric water. Meteoric water derived from precipitation at Earth**'**s surface and is heated in geothermal settings up to 350 $^{O}$C (Schwarzenbach & Steele-MacInnis, 2020).

## 4. Conclusions

Mineralogical properties of common opal from Lop Buri show SG of samples ranging within 1.820-1.950 (1.87 on average). RI varied within 1.43-1.44. Most samples are inert in short-wave and long-wave ultraviolet radiation.

Rock samples (rhyolite) are of silicic composition and show sub-alkaline magma series. Opals are genetically related to their host rocks. Opal is a secondary mineral filling in the cavities of host rock. The initial silica required for opal formation may have been infiltrated through the underlying high-silica volcanic rock and precipitated in the hollow from fluids. From the SEM results, the fluid was hydrothermal. From XRD results, opal samples were opal-CT and showed morphology with fibrous/platelet/tablet texture, and the XRD pattern showed the characteristic diffraction line of the cristobalite-tridymite-type paracrystalline structure identifying volcanic source, and distinguished a complex opal with complex broad group of three peaks centered on 4.1 Å and a sharp reflection at 2.5 Å. The **"**complex**"** samples had elevated contents of metal impurities. Then, the mineral textures and forms suggest that the precipitation occurred at a low temperature (up to 170 $^{O}$C). Opal samples were found at surface. Thus, from other reasons, the type of hydrothermal fluid was meteoric water.

## Acknowledgements

The authors are very grateful to all staff of Department of Geological Sciences, Faculty of Science, Chiang Mai University, the Synchrotron Light Institute (Thailand) and Faculty of Science and Technology, Chiang Mai Rajabhat University for helping us with field equipment and chemical analysis in their laboratory.

## References

Barr, S. M., & Cooper, M. A. (2013). Late Cenozoic basalt and gabbro in the subsurface in the Phetchabun basin, Thailand: Implications for the Southeast Asian Volcanic Province. *Journal of Asian Earth Sciences, 76*, 169-184.

Caucia, F., Marinoni, L., Leone, A., & Ghisoli, C. (2015). New physical, geochemical and gemological data of opals from Acari Mine (Arequipa Department, Peru). *Neues Jahrbuch Für Mineralogie–Abhandlungen, 192*(1), 73-84.

Chauviré, B., Rondeau, B., Alexandre, A., Chamard-Bois, S., La, C., & Mazzero, F. (2019). Pedogenic origin of precious opals from Wegel Tena (Ethiopia): Evidence from trace elements and oxygen isotopes. *Applied Geochemistry, 101*, 127-139.

Chauviré, B., Rondeau, B., & Mangold, N. (2017). Near infrared signature of opal and chalcedony as a proxy for their structure and formation conditions. *European Journal of Mineralogy, 29*(3), 409-421.

Curtis, N. J., Gascooke, J. R., Johnston, M. R., & Pring, A. (2019). A review of the classification of opal with reference to recent new localities. *Minerals, 9*(5), 299.

Devès, G., Perroux, A., Bacquart, T., Plaisir, C., Rose, J., Jaillet, S., . . . Maire, R. (2012). Chemical element imaging for speleothem geochemistry: Application to a uranium-bearing corallite with aragonite diagenesis to opal (Eastern Siberia, Russia). *Chemical Geology, 294*, 190-202.

Gaillou, E., Delaunay, A., Rondeau, B., Bouhnik-le-Coz, M., Fritsch, E., Cornen, G., & Monnier, C. (2008). The geochemistry of gem opals as evidence of their origin. *Ore Geology Reviews, 34*(1-2), 113-126.

Irvine, T. N., & Baragar, W. (1971). A guide to the chemical classification of the common volcanic rocks. *Canadian Journal of Earth Sciences, 8*(5), 523-548.

Janyawanich, C. (1987). The research of industrial applications of bentonite (in Thai). Bangkok, Thailand: Department of Mineral Resource.

Jungyusuk, N., & Suriyachai, P. (1987). Geology on Ban Maha Pho, King Ampher Sri Thep, Ban Paniat and Amphoe Chai Badan. *Geology on Ban Maha Pho, King Ampher Sri Thep, Ban Paniat and Amphoe Chai Badan*.

Luo, J., Liu, X. F., & Yang, X. X. (2016). Comparative analysis of the characteristics of australian opal and ethiopian opal. *Superhard Material Engineering, 28*, 50-57.

Marlow, F., Sharifi, P., Brinkmann, R., & Mendive, C. (2009). Opals: Status and prospects. *Angewandte Chemie International Edition, 48*(34), 6212-6233.

Meier, M., Ungerer, J., Klinge, M., & Nirschl, H. (2018). Synthesis of nanometric silica particles via a modified Stöber synthesis route. *Colloids and Surfaces A*: *Physicochemical and Engineering Aspects, 538*, 559-564.

Moxon, T. (1996). *Agate*: *Microstructure and possible origin*. Middlesex, England: Terra Publications.

Rondeau, B., Mazzero, F., Bekele, E., Gauthier, F., & Fritsch, E. (2009). New play-of-color opal from Welo, Ethiopia. *Gems and Gemology*: *The Quarterly Journal of the Gemological Institute of America, 45*(1), 59.

Schwarzenbach, E. M., & Steele-MacInnis, M. (2020). Fluids in submarine mid-ocean ridge hydrothermal settings. *Elements*: *An International Magazine of Mineralogy, Geochemistry, and Petrology, 16*(6), 389-394.

Vona, A., & Romano, C. (2013). The effects of undercooling and deformation rates on the crystallization kinetics of Stromboli and Etna basalts. *Contributions to Mineralogy and Petrology, 166*, 491-509.

Vysotskiy, S. V., Ignatiev, A. V., Khlestunova, A. G., Velivetskaya, T. A., & Okrugin, A. S. (2013). Peculiarities of the oxygen isotope ratio in precious opals. *Russian Journal of Pacific Geology, 7*, 427-430.

Vysotsky, S. V., Barkar, A. V., Kuryavy, V. G., Chusovitin, E. A., Karabtsov, A. A., & Safronov, P. P. (2010). Hydrothermal noble opal: Structure and genesis. *Geology of Ore Deposits, 52*, 815-820.

Watkins, J., Manga, M., Huber, C., & Martin, M. (2009). Diffusion-controlled spherulite growth in obsidian inferred from $H_2O$ concentration profiles. *Contributions to Mineralogy and Petrology, 157*, 163-172.

Wilson, M. J. (2014). The structure of opal-CT revisited. *Journal of Non-Crystalline Solids, 405*, 68-75.